CFD Investigation of the Impacts of Variation in Geometry of Twisted Tape on Heat Transfer and Flow Characteristics of Water in Tubes

Taiwo O. Oni [1, 2] and Manosh C. Paul [1]

[1] Systems, Power and Energy Research Division, School of Engineering
University of Glasgow, Glasgow G12 8QQ, UK
[2] Mechanical Engineering Department, Faculty of Engineering
Ekiti State University, Ado-Ekiti, Nigeria
*Correspondence: Manosh.Paul@glasgow.ac.uk, tooni1610@yahoo.com, Tel.: +234(0)803 621 7934

Abstract

In this research paper, the influence of variations in geometry of tape insert on thermal performance and flow characteristics of water inside tubes is investigated by means of computational fluid dynamics (CFD). The tape considered is alternate-axis triangular cut twisted tape. The perimeter of the cuts on the tape, the pitch of the tape and the width of the tape were varied. Turbulent flow is considered and uniform heat flux is imposed on the walls of the tubes. RNG $\kappa - \varepsilon$ turbulence model is selected for the simulations and RANS equations are applied to render the Navier-Stokes equations tractable. The findings of the investigations indicated that the thermal performance of all the tubes fitted with twisted tape is better than that of the tube without twisted tape, and also that the performance is influenced by the geometry of the twisted tape. In particular, the thermal performance diminishes as the tape pitch increases but it is augmented by an increase in the size of the cuts on the tape and an increase in the width of the tape.

Key words: Thermal performance, geometry, turbulence model, heat transfer, simulation.

Nomenclature

Roman symbols

$C_{1\varepsilon}$, $C_{2\varepsilon}$, C_{μ}:	Model constant
E:	Total energy (J)
D:	Diameter of tube (m)
f:	Friction factor
g:	Gravitational acceleration (m/s^2)
G_{κ}:	Generation of turbulence kinetic energy due to the mean velocity gradients
G_{ω}:	Generation of specific dissipation rate
h:	Heat transfer coefficient $(W/m^2.K)$
I:	Turbulence intensity
k:	Thermal conductivity $(W/m.K)$
k_{eff}	Effective thermal conductivity $(W/m.K)$
L:	Length of tube (m)
Nu:	Nusselt number
p:	perimeter of cut on twisted tape (m)
P:	Pressure (N/m^2)
Re:	Reynolds number
R_{ε}:	Term which is related to the mean strain and turbulence quantities
T:	Temperature (K)
u:	Mean velocity (m/s)
$\vec{u}$:	Velocity vector (m/s)
w:	Width of twisted tape (m)
x:	Axial coordinate (m)
y:	Pitch of twisted tape

Greek symbols

α_{κ}, α_{ε}:	Inverse Prandtl number for κ, ε
ε:	Dissipation rate of turbulent kinetic energy (m^2/s^3)
η:	Thermal performance factor
ι :	Unit tensor
κ:	Turbulent kinetic energy (m^2/s^2)
μ:	Dynamic viscosity (kg/ms)
μ_{eff}:	Effective dynamic viscosity (kg/ms)
μ_t:	Turbulent dynamic viscosity (kg/ms)
ρ:	Density (kg/m^3)
σ_{κ}, σ_{ε}, σ_{ω}:	Prandtl number for κ, ε, ω
$\bar{\bar{\tau}}$:	Stress tensor (N/m^2)
ω:	Specific dissipation rate (K^{-1})

1. Introduction

Heat energy is indispensable to the survival of man and this has made him to be occupied by the quest for its effective utilization in industrial and domestic activities [1]. As a matter of fact, the application of heat energy is becoming critical in areas such as refrigeration plant, solar water heaters, electronics thermal management, heat pipes, aerospace, automobiles, and medicines [2-4]. In order to reduce the aggregate financial resources that go into producing heat energy, it has become necessary to design heat transfer equipment that are more efficient in performance, and at the same time are able to reduce energy and cost. In this regard, heat transfer enhancement becomes important [5].

Because of their simplicity and no need for external power, passive methods of heat transfer enhancement have shown much potential and found unlimited applications. These passive methods incorporate additional devices such as twisted tape inserts and displaced enhancement devices, or make use of geometrical modifications such as extended surfaces and rough surfaces to the flow channel [6, 7]. The simple configuration, low maintenance cost and easy installation of twisted tape has made its use a popular choice to enhance heat transfer [3, 8]. Twisted tapes which are properly designed offer the promotion of heat transfer with a reasonable penalty in pressure drop which ultimately yields savings in energy and cost [9, 10].

Studies on the enhancement of heat transfer have been in progress for some times to yield better results for performance of heat exchangers. One of the early works in this regard was experimentally carried out by Kreith and Margolis [11] on turbulent flow through tubes induced with twisted tape and obtained a significant enhancement in heat transfer over that in the plain tube.

Gupte and Date [12] numerically evaluated the Nusselt number and friction factor of swirl flow generated by twisted tape of twist ratios ∞, 5.3, 5.04, and 2.66 in annuli and reported an increase in Nusselt number and friction factor in the induced tube over those in the plain tubes.

The influences of twisted tape insertion on heat transfer and flow characteristics in a concentric double pipe heat exchanger were experimentally studied by Noothong et al. [13]. The results revealed that the heat transfer for the tube induced with twisted-tape of pitches of 5 and 7 were 188% and 159% respectively of those for the plain tube.

Chang et al. [14], in their work on turbulent heat transfer and pressure drop in tube fitted with serrated twisted tape, made it known that the tube fitted with serrated twisted tape produced a better heat transfer

enhancement than the tube fitted with smooth-walled twisted tape. The heat transfer augmentation attributed to serrated twisted tape was found to be about 1.25 to 1.67 times that in the tube fitted with smooth twisted tape and 2.5 – 4.8 times that in the plain tube.

Chiu and Jang [15] examined numerical and experimental analyses for thermal-hydraulic characteristics inside a circular tube with different tape inserts. They discovered that the heat transfer enhancement by the longitudinal strip insert without hole and longitudinal strip insert with holes were up to 116% and 118% respectively of that in the plain tube.

Murugesan et al. [16] fabricated a trapezoidal-cut twisted tape, and experimentally discussed the heat transfer and pressure drop characteristics of turbulent flow in a circular tube fitted with the twisted tape. They observed a significant increase in heat transfer coefficient and friction factor for the tape with trapezoidal-cut. The Nusselt number for the trapezoidal-cut twisted tape was 1.72 to 2.85 times that of plain tube.

In another work, Murugesan et al. produced a twisted tape with square cuts [17] and performed an experimental investigation with it on a double pipe heat exchanger. They concluded that the Nusselt number for the tube induced with square-cut twisted tape of twist ratios 2.0, 4.4 and 6.0 were 1.08, 1.067 and 1.055 respectively times those of the tubes induced with plain twisted tape, and their friction factors were 1.09, 1.12 and 1.15 respectively times those of the tube with plain twisted-tape insert.

Cui and Tian [18] published their findings on the numerical and experimental work done on heat transfer characteristics and pressure drop of air in a circular tube induced individually with edgefold-twisted tape inserts and classic spiral-twisted-tape inserts of the same twist ratio. Their results showed that the Nusselt number of the tube with edgefold-twisted tape inserts was 1.04 to 1.09 times that with spiral-twisted tape inserts, and the friction factor of the tube with edgefold-twisted tape inserts was 1.087 to 1.74 times that of the spiral-twisted tape inserts.

According to the observation of Guo et al. [19], the thermal performance of a tube fitted with a centre-cleared twisted tape can be augmented up to 1.2 times of a tube fitted with a plain twisted tape. The numerical analysis of heat transfer and fluid flow through a round tube fitted individually with triple or quadruple twisted tapes was presented by Zhang et al. [20], and they concluded that the Nusselt number of the tube with triple twisted tape and quadruple twisted tape were significantly higher than that of the plain tube.

Through the publication of Salman et al. [21], it was discovered that heat transfer in a plain tube can be enhanced by inserting an alternate-axis twisted tape or a plain twisted tape into the plain tube. The heat transfer for turbulent flow in a tube fitted with single, double, triple and quadruple twisted tape inserts was experimentally examined by Chokphoemphun et al. [22], and they concluded that the Nusselt number for the induced tubes was 15% to 112% higher that for the plain tube.

The above-mentioned works indicated that the heat transfer produced by the tubes induced with plain twisted tapes or modified twisted tapes is higher than those produced in the tubes without a twisted tape. However, the works did not provide a comprehensive analysis of the impacts which the variation in the geometry of the tape will have on thermal-hydraulic performance of the flow systems. Hence, the present work numerically explores the effects of the variations in tape pitch, tape width, and size of cuts on the tape on heat transfer and flow characteristics of water in tubes induced with alternate-axis triangular cut twisted tape.

2. Physical models

Eight different models are considered in this study. One of them is a plain tube while the others are tubes induced with a modified twisted tape. The tube is depicted in **Fig. 1**(a) and its diameter (D) and length (L) are 19mm and 1000mm respectively. In **Fig. 1** (b), the width and the pitch of the twisted tape are represented by w and y respectively. The tapes have alternate axes and equilateral triangular cuts are made on them, and

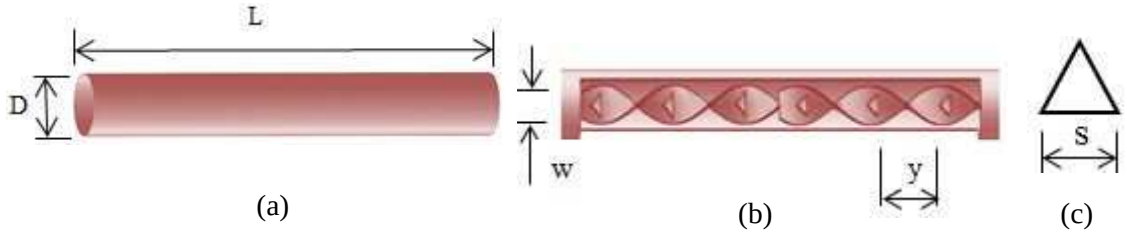

Fig. 1. (a) Physical model for plain tube, (b) physical model for plain tube induced with twisted tape, and (c) triangular cut on the twisted tape.

hence the tape is referred to in this work as alternate-axis triangular cut twisted tape (ATCT). The triangular cut is shown in **Fig. 1**(c). As presented in **Table 1**, the individual tapes in the seven induced tubes are ATCT, $ATCT_{w1}$, $ATCT_{w2}$, $ATCT_{p1}$, $ATCT_{p2}$, $ATCT_{y1}$, and $ATCT_{y2}$. The tape ATCT is the reference tape for the present investigation. This means that all the other six tapes are obtained from the ATCT by varying its geometry. The geometry of the tapes are different from one another in the width (w), pitch (y), length (s) of a side of the triangular cut, and perimeter (p) of the cut. The physical models upon which the investigation is

conducted in the present work, as shown in **Table 1**, are PT, TATCT, $TATCT_{w1}$, $TATCT_{w2}$, $TATCT_{p1}$, $TATCT_{p2}$, $TATCT_{y1}$, and $TATCT_{y2}$.

Table 1
Description of the various geometries of the alternate-axis triangular cut twisted tape and various physical models.

Tape	Geometry				Physical model
	w (mm)	*y* (mm)	*s* (mm)	*p* (mm)	
					PT
ATCT	18	54	11.42	34.26	TATCT
$ATCT_{w1}$	15	54	11.42	34.26	$TATCT_{w1}$
$ATCT_{w2}$	13	54	11.42	34.26	$TATCT_{w2}$
$ATCT_{p1}$	18	54	9.00	27.00	$TATCT_{p1}$
$ATCT_{p2}$	18	54	6.00	18.00	$TATCT_{p2}$
$ATCT_{y1}$	18	36	11.42	34.26	$TATCT_{y1}$
$ATCT_{y2}$	18	72	11.42	34.26	$TATCT_{y2}$

3. Governing equations and assumptions

The following assumptions are made for the governing equations:

- The fluid flow is steady.
- The fluid flow is incompressible.
- Viscous dissipation is negligible.
- Compression work is negligible.
- Thermal radiation and chemical reaction are negligible.

Consequent upon the above assumptions, the governing equations for the models can be expressed [23, 24] as:

continuity equation:

$$\frac{\partial \rho}{\partial t} + \nabla.(\rho \vec{u}) = 0 \tag{1}$$

momentum equation:

$$\frac{\partial (\rho \vec{u})}{\partial t} + \nabla.(\rho \vec{u}\vec{u}) = \rho g - \nabla P + \nabla.(\bar{\bar{\tau}}) \tag{2}$$

energy equation:

$$\frac{\partial (\rho E)}{\partial t} + \nabla.\left(\vec{u}(\rho E + P)\right) = \nabla.\left(k_{eff}\nabla T + \left(\bar{\bar{\tau}}_{eff}.\vec{u}\right)\right) \tag{3}$$

where

$$\bar{\bar{\tau}}_{eff} = \mu\left((\nabla\vec{u} + \nabla\vec{u}^{T}) - \frac{2}{3}\nabla.\vec{u}\iota\right) \tag{4}$$

4. Turbulence modelling

Different turbulence models are used to ascertain the suitability of each of them for the simulations. They are RNG $\kappa - \varepsilon$, standard $\kappa - \varepsilon$, and standard $\kappa - \omega$ models.

4.1. RNG $\kappa - \varepsilon$ model

The renormalization group (RNG) $\kappa - \varepsilon$ model, derived by Yakhot et al. [25], is based on model transport equations for the turbulence kinetic energy (κ) and turbulence dissipation rate (ε) [23] viz

$$\frac{\partial}{\partial t}(\rho\kappa) + \frac{\partial}{\partial x_i}(\rho\kappa u_i) = \frac{\partial}{\partial x_j}\left[\alpha_\kappa \mu_{eff}\frac{\partial\kappa}{\partial x_j}\right] + G_k - \rho\varepsilon \tag{5}$$

$$\frac{\partial}{\partial t}(\rho\varepsilon) + \frac{\partial}{\partial x_i} = \frac{\partial}{\partial x_j}\left[\alpha_\varepsilon \mu_{eff}\frac{\partial\varepsilon}{\partial x_j}\right] + C_{1\varepsilon}\frac{\varepsilon}{\kappa}G_k - C_{2\varepsilon}\,\rho\,\frac{\varepsilon^2}{\kappa} - R_\varepsilon \tag{6}$$

The model constants are $C_{1\varepsilon} = 1.42$, $C_{2\varepsilon} = 1.68$, $C_\mu = 0.0845$, $\sigma_\kappa = 0.7194$ and $\sigma_\varepsilon = 0.7194$ [23].

4.2. Standard $\kappa - \omega$ model

The standard $\kappa - \omega$ model is based on the Wilcox $\kappa - \omega$ model[26]. It is based on transport equations for the turbulence kinetic energy (κ) and the specific dissipation rate (ω) [23] which are given as

$$\frac{\partial}{\partial t}(\rho\kappa) + \frac{\partial}{\partial x_i}(\rho\kappa u_i) = \frac{\partial}{\partial x_j}\left[(\mu + \frac{\mu_t}{\sigma_\kappa})\frac{\partial\kappa}{\partial x_j}\right] + G_k - \beta_1\kappa\omega \tag{7}$$

$$\frac{\partial}{\partial t}(\rho\omega) + \frac{\partial}{\partial x_i}(\rho\omega u_i) = \frac{\partial}{\partial x_j}\left[\left(\mu + \frac{\mu_t}{\sigma_\omega}\right)\frac{\partial\omega}{\partial x_j}\right] + G_\omega - \beta_2\omega^2 \tag{8}$$

The model constants are $\beta_1 = \beta_2 = 0.072$.

4.3. Standard $\kappa - \varepsilon$ model

The standard $\kappa - \varepsilon$ model is a turbulence model proposed by Launder and Spalding [27] and it is based on turbulent kinetic energy (κ) and turbulence dissipation rate (ε). Its transport equations are given [23] as

$$\frac{\partial}{\partial t}(\rho\kappa) + \frac{\partial}{\partial x_i}(\rho\kappa u_i) = \frac{\partial}{\partial x_j}\left[\left(\mu + \frac{\mu_t}{\sigma_\kappa}\right)\frac{\partial\kappa}{\partial x_j}\right] + G_k - \rho\varepsilon \tag{9}$$

$$\frac{\partial}{\partial t}(\rho\varepsilon) + \frac{\partial}{\partial x_i}(\rho\varepsilon u_i) = \frac{\partial}{\partial x_j}\left[\left(\mu + \frac{\mu_t}{\sigma_\varepsilon}\right)\frac{\partial \varepsilon}{\partial x_j}\right] + C_{1\varepsilon}\frac{\varepsilon}{\kappa}G_k - C_{2\varepsilon}\rho\frac{\varepsilon^2}{\kappa} \quad (10)$$

The model constants are $C_{1\varepsilon} = 1.44$, $C_{2\varepsilon} = 1.92$, $C_\mu = 0.09$, $\sigma_\kappa = 1.0$ and $\sigma_\varepsilon = 1.3$ [23].

5. Boundary conditions

Appropriate boundary conditions are necessary for solving the set of non-linear governing equations and therefore considered in the numerical simulations. At the pipe inlet, temperature $T_i = 301K$, diameter $D = 0.019m$, velocity (v) derived by $v = Re.\mu/\rho.D$ (where Re is the Reynolds number), and turbulence intensity $I = 0.16/Re^{0.125}$ were set. A uniform heat flux, $-k\left(\frac{\partial T}{\partial x}\right)_{D/2}$, is imposed on surface of the tube wall, and it is also subjected to a no-slip condition, i.e. $u_i = u_j = u_k = 0$.

6. Numerical method

The finite volume method of Fluent was used to discretize the governing equations. Through the second order upwind discretization scheme, Taylor series expansion was used to compute the unknown quantities at the cell faces. As a way of incorporating the effects of pressure into the solution for the momentum equation, the Semi Implicit Pressure Linked Equations algorithm was used to couple the velocity and pressure. To account for the low Reynolds number and the near wall flow, an enhanced wall treatment was adopted for the simulation. The iterative solution of the equations was obtained by the Fluent software [23, 24, 28].

7. Convergence and grid independency

The need to confirm the accuracy of the numerical solutions necessitated the grid independence tests that were conducted for the domains. The different grids used for each domain is provided in **Table 2**. In conducting the grid independence test, the temperature for $Re = 20000$ across the cross-section at the exit of the domains was extracted and the results are shown in **Fig. 2**. It can be seen from the figure that the grid with cell 512420 or 717388 can be adopted for the PT (**Fig. 2** (a)). The grid with cell 2515756 or 3018907 is suitable for the TATCT (**Fig. 2** (b)). For the $TATCT_{w1}$ (**Fig. 2** (c)), the grid with cell 2449381 or 3184196 is appropriate. The grid with cell 2405132 or 3126671 is fit for the $TATCT_{w2}$ (**Fig. 2** (d)). The $TATCT_{p1}$ (**Fig. 2** (e)) can adopt the grid with cell 2522878 or 3279741. For the $TATCT_{p2}$ (**Fig. 2** (f)), the grid with cell

Table 2
Independency of grid

Domain	Cell		
PT	461178	512420	717388
TATCT	1658638	2515756	3018907
$TATCT_{w1}$	1714567	2449381	3184196
$TATCT_{w2}$	1683592	2405132	3126671
$TATCT_{p1}$	1766015	2522878	3279741
$TATCT_{p2}$	1770542	2529346	3288150
$TATCT_{y1}$	1752274	2503249	3254223
$TATCT_{y2}$	1761029	2515756	3270483

2529346 or 3288150 can be adopted. The grid with cell 2503249 or 3254223 is suitable for the $TATCT_{y1}$ (**Fig. 2**(g)). For the $TATCT_{y2}$ (**Fig. 2** (h)), the grid with cell 2515756 or 3270483 can be adopted. Considering solution precision as well as the time for convergence, the grids with cells 512420, 2515756, 2449381, 2405132, 2522878, 2529346, 2503249 and 2515756 were adopted for the PT, TATCT, $TATCT_{w1}$, $TATCT_{w2}$, $TATCT_{p1}$, $TATCT_{p2}$, $TATCT_{y1}$ and $TATCT_{y2}$ respectively.

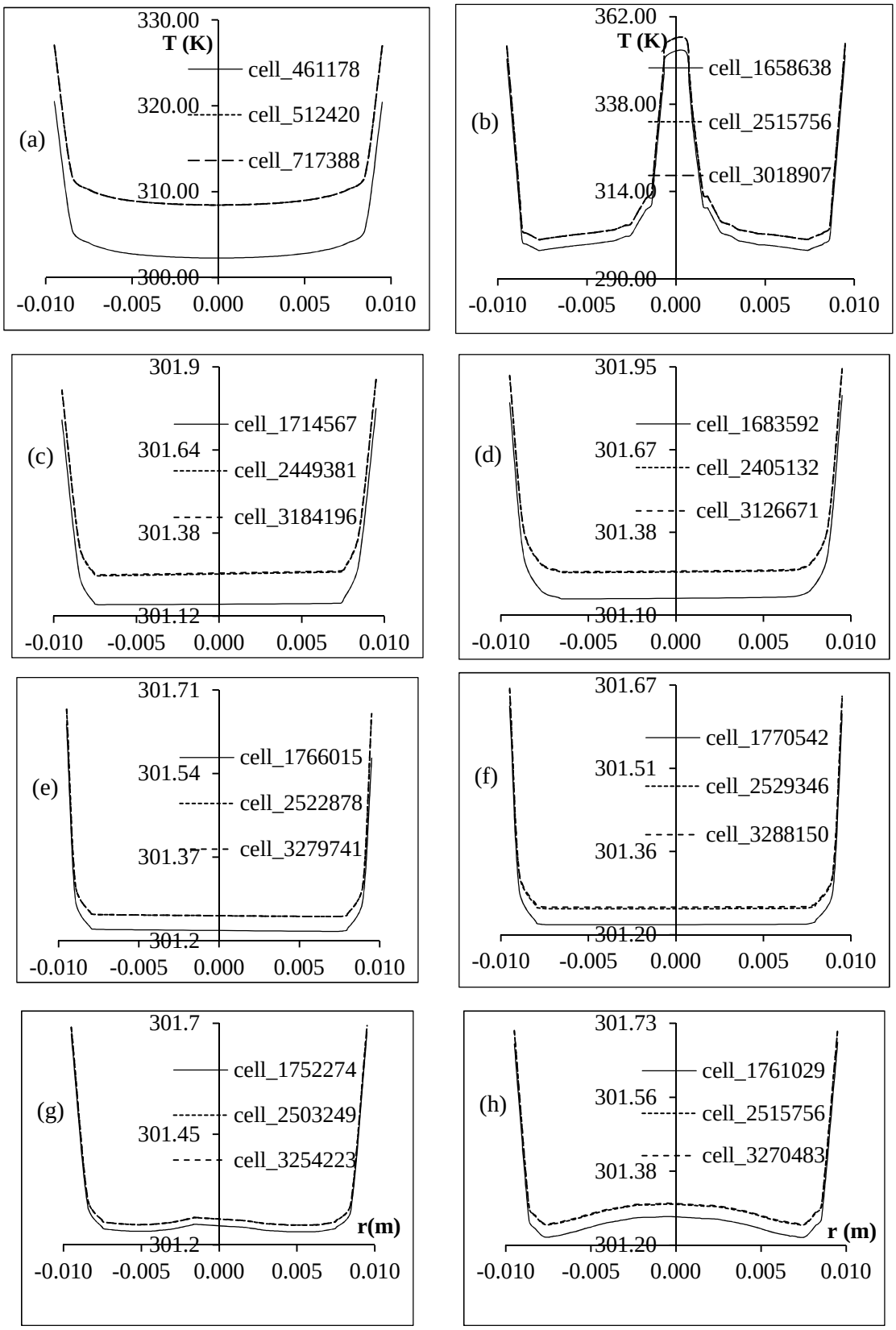

Fig. 2. Temperature across the cross-section at the exit of (a) PT, (b) TATCT, (c) TATCTw1, (d) $TATCT_{w2}$, (e) $TATCT_{p1}$, (f) $TATCT_{p2}$, (g) $TATCT_{y1}$ and (h) $TATCT_{y2}$ for $Re = 20000$ for different grids.

8. Assessment of different turbulence models

Three turbulent models were assessed to know the most suitable one for the simulations. To carry out the assessment, the Nusselt number obtained with the standard $\kappa - \varepsilon$, RNG $\kappa - \varepsilon$ and standard $\kappa - \omega$ turbulence models for the plain tube (PT) was validated with the Gnielinski correlation [29] and the experimental results of Seemawute and Eiamsa-ard [30].

As shown in **Fig. 3**, the Nusselt number for the RNG κ-ε model agrees with the experimental results of Seemawute and Eiamsa-ard with a maximum deviation of 4.12%, but it agrees with the Gnielinski correlation with a maximum deviation of 6.25%. The maximum deviation for each of the standard $\kappa - \omega$ and

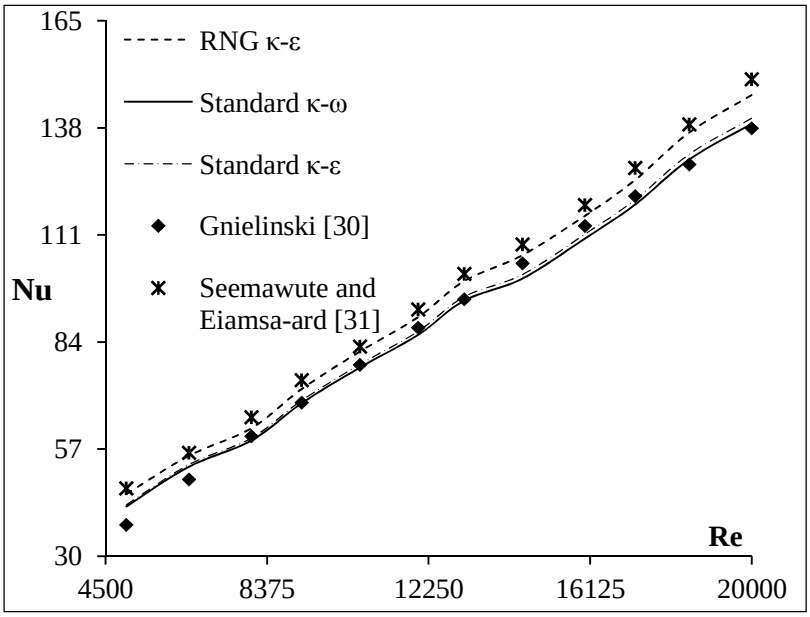

Fig. 3. Assessment of different turbulent models.

standard $\kappa - \varepsilon$ models is 7.67% when compared with the Gnielinski correlation, but it is in agreement with the Seemawute and Eiamsa-ard experimental results with a maximum deviation of 8.74%. It is evident that the RNG $\kappa - \varepsilon$ model predicts the numerical results better than the other turbulence models. Therefore, it is selected to perform all the other numerical simulations in this work.

9. Discussion of computational results

9.1. Velocity vector

The velocity vectors for the various models at the same location of 0.866m are depicted in **Fig. 4**. The PT (frame a) is not induced with tape and therefore swirl flow is not generated in it. The velocity vectors for the variations in width w = 18mm, 15mm and 13mm are shown in frames (b), (c) and (d) respectively. It is seen

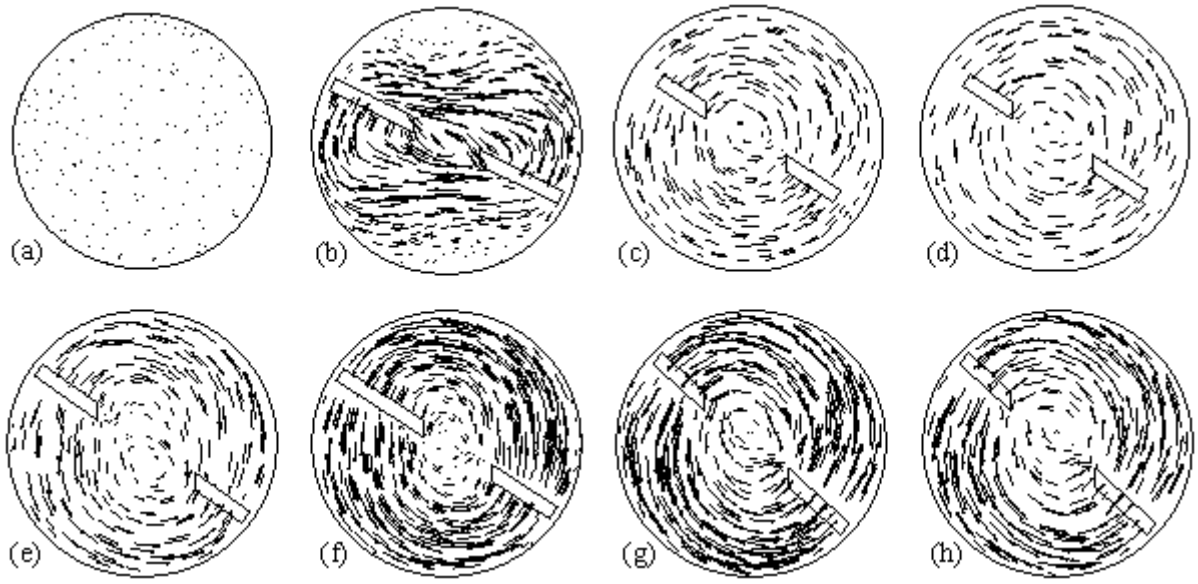

Fig. 4. Velocity vector of (a) PT, (b) TATCT, (c) $TATCT_{w1}$, (d) $TATCT_{w2}$, (e) $TATCT_{p1}$, (f) $TATCT_{p2}$, (g) $TATCT_{y1}$ and (h) $TATCT_{y2}$.

that when w = 15mm (frame c), the velocity near the wall is smaller than when w = 18mm (frame b), which means a weaker fluid mixing near the wall when w = 15mm. A further reduction in swirl is observed as the width is reduced to 13mm (frame d). The velocity vectors for the variations in the size of the cut on the tape perimeter from p = 34.26mm to 27mm, and then to 18mm are shown in frames (b), (e) and (f) respectively. From these, it can be seen that the swirl in the tube with the tape cut of size p = 34.26mm (frame b) is stronger than that with p = 27mm (frame e) while the swirl in the tube with p = 18mm (frame f) is weaker than that with cut p = 27mm (frame e). This means that as the size of the cut reduces the swirls near the wall diminishes. The velocity vectors for the variations in tape pitch y = 54mm, 36mm and 72mm are shown in frames (b), (g) and (h) respectively. The swirl in the tube with the largest tape pitch y = 72mm (frame h) is the weakest while the strongest swirl is obtained in the tube with the smallest tape pitch of 36mm (frame g).

9.2. Turbulent kinetic energy

The effect which the variations in the geometry of the tape have on the turbulent kinetic energy is displayed in **Fig. 5**. In the PT (frame a), the maximum turbulent kinetic energy (TKE) occurs at the wall of the tube. This is due to the minimum velocity that resides at the wall of the PT. When the tube is induced with a tape of width 18mm (frame b), the velocity between the tape and the tube wall increases. Consequently, the TKE between the tape and the edge of the tube reduces. As the tape width is decreased to 15mm (frame c) and 13mm (frame d), the TKE between the edge of the tape and the wall of the tube increases as a result of the

decrease in the velocity near the wall. Comparison of the TKE for the size of the cut of perimeter p = 34.26mm (frame b), 27mm (frame e) and 18mm (frame f) shows that the TKE near the wall of the domain when p = 34.26mm is higher than that when p = 27mm, and there is a further increase in the TKE when p = 18mm. The reason adduced for this is the velocity between tube wall and the edge of the tape which reduces

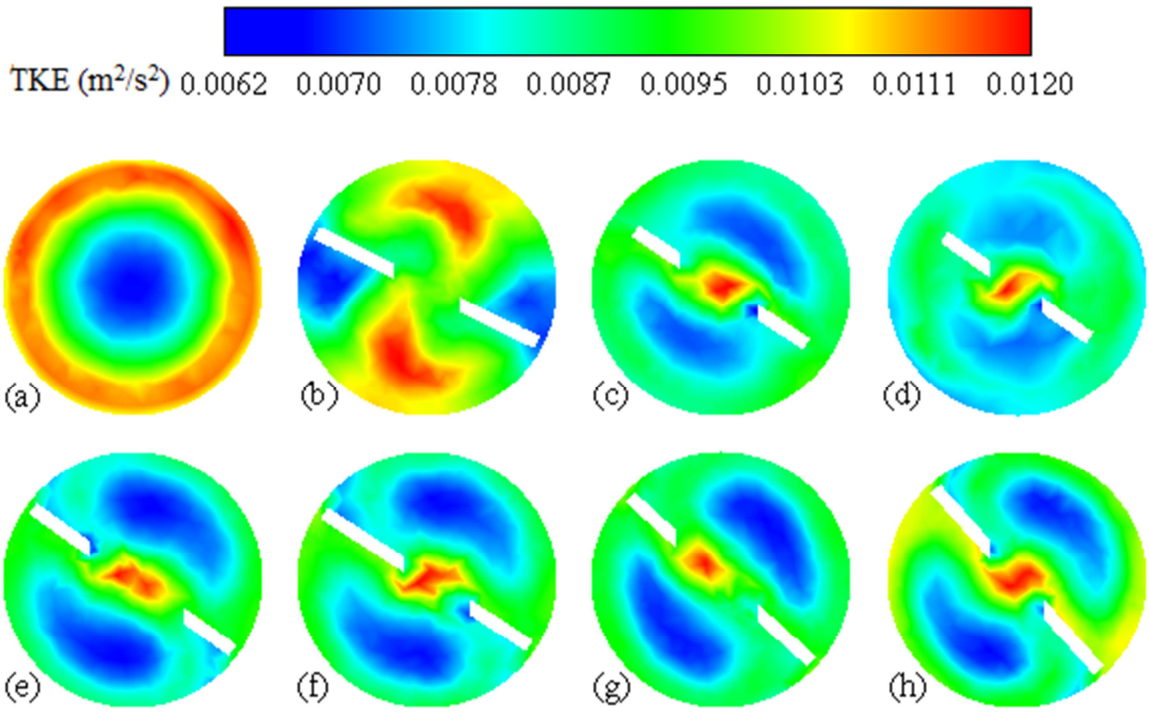

Fig. 5. Contour plots of turbulent kinetic energy of (a) PT, (b) TATCT, (c) $TATCT_{w1}$, (d) $TATCT_{w2}$, (e) $TATCT_{p1}$, (f) $TATCT_{p2}$, (g) $TATCT_{y1}$ and (h) $TATCT_{y2}$.

as the size of cut is reduced. When the pitch of the tape is varied from y = 54mm (frame b) to 36mm (frame g), the TKE between the tube wall and the tape decreases, whereas there is an increase in the TKE as the tape pitch is increased from 36mm (frame g) to 72mm (frame h).

9.3. Influence of the variations in the tape geometries on heat transfer

The heat transfer is expressed in terms of Nusselt number (Nu). The effects of the variations in the geometries of the tape on the heat transfer are presented in **Fig. 6**. As mentioned previously in §2, the tape ATCT is the reference tape for the investigation. As seen in **Fig. 6**, the Nusselt number for the tube fitted with the ATCT (that is, TATCT) is significantly higher than that for the plain tube (PT).

From **Fig. 6** (a), the Nusselt number for the tubes with tape cut of size or perimeter p = 27mm ($TATCT_{p1}$) and 18mm ($TATCT_{p2}$) are 2.5% and 7.9% respectively lower than that for the tape with p = 34.26mm

(TATCT). This means that the Nusselt number decreases with the decrease in the size or perimeter of the tape cut. The reason behind this is that once a cut is made on the surface of the twisted tape, the cut adds to the swirls in the tube, thereby increasing the disturbance to the flow between the wall of the tube and the

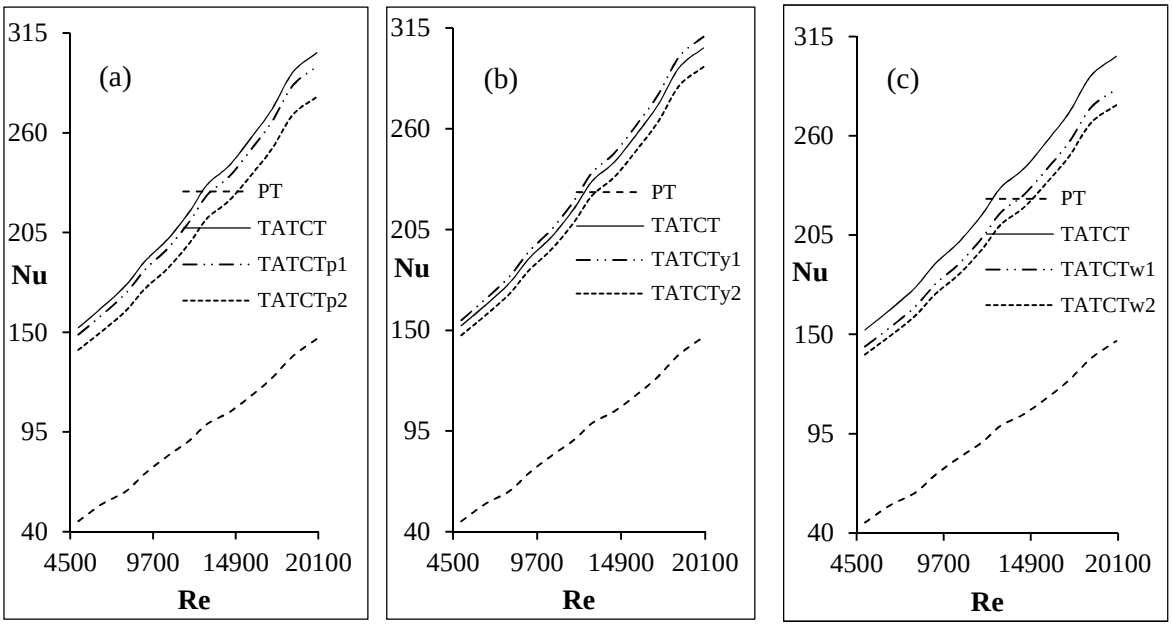

Fig. 6. Effect of variations in (a) size of tape cut, (b) tape pitch, and (c) tape width on Nusselt number vs. Reynolds number.

edge of the tape. The smaller the perimeter of the cut, the less the effect which this effect has on the heat transfer. The tape with smallest perimeter of cut therefore imparts lowest disturbance to the flow and thus has the lowest Nusselt number.

It is revealed in **Fig. 6** (b) that the Nusselt number increases when the tape pitch decreases from y = 54mm (TATCT) to 36mm ($TATCT_{y1}$) but decreases when the pitch increases to 72mm ($TATCT_{y2}$). The increase in the heat transfer at smaller tape pitch is attributed to a stronger swirl and longer flowing path which is consequent upon the reduction in the tape pitch. The tape with y = 36mm ($TATCT_{y1}$) enhances the heat transfer up to 2.1% over that of the tape with y = 54mm (TATCT), but the tape with y = 72mm ($TATCT_{y2}$) suffers a reduction in heat transfer of 3.4% of the tape with y = 54mm (TATCT).

The discovery from **Fig. 6** (c) is that the Nusselt number with tape geometry of width w = 15mm ($TATCT_{w1}$) and 13mm ($TATCT_{w2}$) are 6.1% and 8.9% respectively lower than that of w = 18mm (TATCT). The inference is that the Nusselt number decreases with increasing tape width. This is because the domain $TATCT_{w2}$ with the largest free space between the tube wall and edge of the tape generates the weakest swirl,

which in turn produces the thickest boundary layer whereas the domain TATCT with the smallest space creates the strongest swirl, resulting in heat transfer that is higher than what is obtained in the other domains.

9.4. Influence of the variations in the tape geometries on friction factor

The effects of the variations in the geometries of the tape on the friction factor are presented in **Fig. 7**. It can be seen from the figure that the TATCT, that is the tube induced with the reference tape ATCT, has a higher friction factor than the PT. This is as a result of flow blockage and swirl from the tape. It is evident in **Fig. 7** (a) that the friction factors of the tube with tape cut of size or perimeter p = 27mm ($TATCT_{p1}$) and 18mm ($TATCT_{p2}$) are lower than that of the tape with p = 34.26mm (TATCT) by 2.3% and 7.5% respectively. The

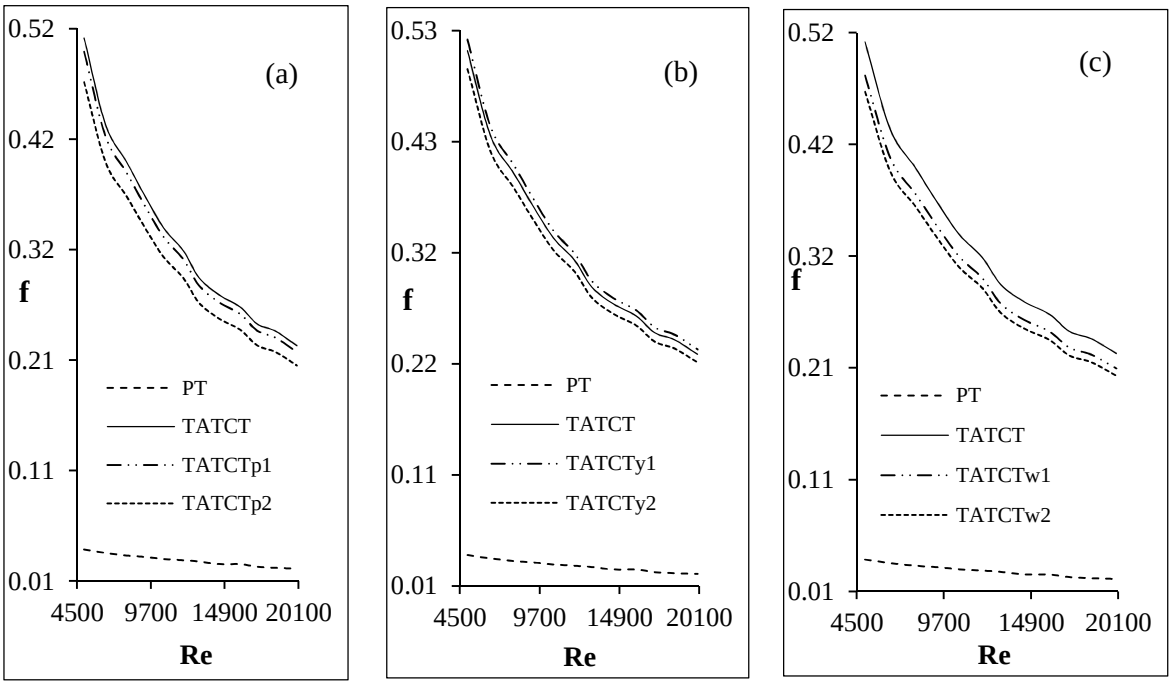

Fig. 7. Effect of variations in (a) size of tape cut, (b) tape pitch, and (c) tape width on friction factor vs. Reynolds number.

indication is that the friction factor decreases as the perimeter of the cut decreases. This is because the tape with large perimeter of cut has a less blocking area. Also, the additional dissipation of pressure of the fluid caused by the fluid disturbance due to the presence of cuts on the tapes resulted in an increase of interaction of the pressure force around a velocity boundary layer.

As depicted in **Fig. 7** (b), the friction factor is increased with the tape pitch decreasing from y = 54mm (TATCT) to 36mm ($TATCT_{y1}$) but decreases when the pitch is increased from 54mm to 72mm ($TATCT_{y2}$).

The friction factors obtained with the tape with y = 36mm and 72mm are 2.2% higher and 3.2% lower respectively than that obtained in the tape with y = 54mm.

From **Fig. 7** (c), it is observed that the friction factor decreases with the reduction of the tape width from w = 18mm (TATCT) to 15mm ($TATCT_{w1}$), and then to 13mm ($TATCT_{w2}$). The value of the friction factor when w = 18mm decreases by 5.9% as compared with that when w = 15mm, but decreases by 8.6% when w = 13mm.

9.5. Influence of the variations in the tape geometries on thermal performance factor

The possibility of a twisted tape in enhancing heat transfer is measured by thermal performance factor (η), and it is defined [31] as

$$\eta = \left(\frac{Nu}{Nu_p}\right)\left(\frac{f}{f_p}\right)^{-1/3} \tag{11}$$

where Nu and Nu_p are the Nusselt number for the induced tube and plain tube respectively, and f and f_p are the friction factor for the induced tube and plain tube respectively.

The effects which the variation in the tape geometry has on thermal performance factor are demonstrated in **Fig. 8**. From **Fig. 8** (a), the thermal performance factor obtained for the tube with the tape cut of size or perimeter p = 27mm ($TATCT_{p1}$) and 18mm ($TATCT_{p2}$) are 1.1% and 3.1% respectively lower than that with p = 34.26mm (TATCT), indicating that the thermal performance increases as the size of the cut increases.

It is observed from **Fig. 8** (b) that the tape with smallest pitch of y = 36mm ($TATCT_{y1}$) produces the highest thermal performance factor, but the smallest thermal performance factor is obtained from the tape with the largest pitch y = 72mm ($TATCT_{y2}$). It is seen from the figure that the thermal performance factor of the tape with y = 36mm ($TATCT_{y1}$) is enhanced up to 1.1% over that of the tape with y = 54mm (TATCT), but the tape with y = 72mm ($TATCT_{y2}$) has its thermal performance factor diminished by 1.3% compared with that of the tape with y = 54mm.

The thermal performance factor as it is affected by a change in the tape width is shown in **Fig. 8** (c). The results reveal that the tapes with the largest width w = 18mm (TATCT) offer the highest thermal performance factor. The thermal performance obtained from the tape with w = 15mm ($TATCT_{w1}$) and

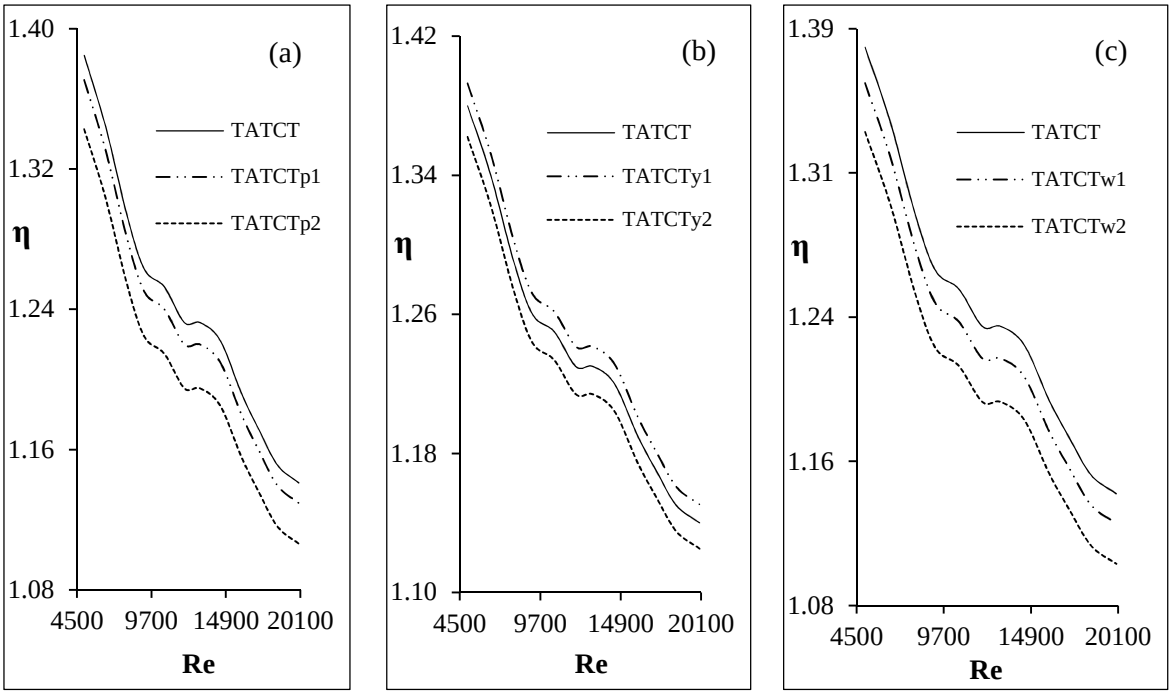

Fig. 8. Effect of variations in (a) size of tape cut, (b) tape pitch, and (c) tape width on thermal performance factor vs. Reynolds number.

13mm ($TATCT_{w2}$) are 1.4% and 3.3% respectively lower than that of the tape with w = 18mm. The applications of the various tape geometries for the enhancement of heat transfer are found to be promising since the thermal performance factors obtained under these conditions are above unity.

10. Conclusion

In this study, the effects of variation in the geometry of tape insert on heat transfer and flow characteristics in tubes are numerically investigated. The various tube designs considered have the geometries of their tape inserts varied in the tape width (13mm ≤ w ≤ 18mm), the tape pitch (36mm ≤ y ≤ 72mm), and the size of the cut on the tapes (18mm ≤ p ≤ 34.26mm). The Reynolds numbers considered for the turbulent flow is 5000 ≤ Re ≤ 20000, and the walls of the tubes are subjected to uniform heat flux.

It was discovered that increasing the size of the cut on the tape is favourable to the flow system as this enhances the thermal performance of the system. In this regard, the domain TATCT (p = 34.26mm) is the best. Moreover, the results revealed that increasing the tape pitch results in the reduction of the thermal performance of the system. Based on this, the domain $TATCT_{y1}$ (y = 36mm) is the best. Furthermore, it was observed that increasing the width of the tape is advantageous as it enhances the thermal performance. Considering this, TATCT (w = 18mm) is the best domain.

Acknowledgement

The financial sponsorship provided for this work by the Ekiti State University Nigeria through a fund from the Tertiary Education Trust Fund Nigeria is gratefully acknowledged.

Literature Cited

1. Jiji LM (2009) Heat Convection, 2nd Edition. New York: Springer Berlin Heidelberg.
2. Manglik RM (2003) Heat Transfer Enhancement In Heat Transfer Handbook, 1st Edition (Bejan A & Kraus AD, Eds). NJ: John Wiley & Sons, Inc.
3. Dewan A, Mahanta P, Raju KS & Kumar PS (2004) Review of Passive Heat Transfer Augmentation Techniques. Proceedings of the Institutions of Mechanical Engineers, Part A: J Power and Energy, 218: 509-527.
4. Lane HJ & Heggs PJ (2005) Extended Surface Heat Transfer - the Dovetail Fin. Appl Therm Eng, 25: 2555-2565.
5. Bergles AE (1999) The Imperative to Enhance Heat Transfer In Heat Transfer Enhancement of Heat Exchangers, (Kakac S, Bergles AE, Mayinger F & Yuncii H, Eds). pp: 13-29. Dordrecht: Kluwer.
6. Webb RL (1987) Enhancement of Single-Phase Heat Transfer In Handbook of Single-Phase Convective Heat Transfer, (Kakac S, Shah RK & Aung W, Eds). NY: John Wiley & Sons Inc.
7. Bergles AE (1998) Techniques to Enhance Heat Transfer In Handbook of Heat Transfer, 3rd Edition (Rohsenow WM, Hartnett JP & Cho YI, Eds). NY: McGraw-Hill.
8. Manglik RM & Bergles AE (1993) Heat Transfer and Pressure Drop Correlations for Twisted -Tape Inserts in Isothermal Tubes: Part II - Transition and Turbulent Flows Transanc ASME J Heat Trans, 115: 890-896.
9. Jaisankar S, Radhakrishnan TK, Sheeba KN & Suresh S (2009) Experimental Investigation of Heat Transfer and Friction Factor Characteristics of Thermosyphon Solar Water Heater System Fitted with Spacer at the Trailing Edge of Left-Right Twisted Tapes. Energy Convers Manage, 50: 2638–2649.
10. Kumbhar DG & Sane NK (2010) Heat Transfer Enhancement in a Circular Tube Twisted with Swirl Flow Generator. In Proceedings of the Third International Conference on Advances in Mechanical Engineering (pp.188-192) January 4-12, Gujarat, India.
11. Kreith F & Margolis D (1959) Heat Transfer and Friction in Turbulent Vortex Flow. Appl Sci Res, Section A, 8: 457-473.

12. Gupte NS & Date AW (1989) Friction and Heat Transfer Characteristics of Helical Turbulent Air Flow in Annuli. Transanc ASME J Heat Trans, 111: 337–344.

13. Noothong W, Eiamsa-ard S & Promvonge P (2006) Effect of Twisted Tape Inserts on Heat Transfer in a Tube. In Second Joint International Conference on Sustainable Energy and Environment (pp.1-5) Bangkok, Thailand.

14. Chang SW, Jan YJ & Liou JS (2007) Turbulent Heat Transfer and Pressure Drop in Tube Fitted with Serrated Twisted Tape. Int J Therm Sci, 46: 506-518.

15. Chiu Y & Jang J (2009) 3D Numerical and Experimental Analysis for Thermal–Hydraulic Characteristics of Air Flow inside a Circular Tube with Different Tube Inserts. Appl Therm Eng, 29: 250-258.

16. Murugesan P, Mayilsamy K, Suresh S & Srinivansan PSS (2009) Heat Transfer and Pressure Drop Characteristics of Turbulent Flow in a Tube Fitted with Trapezoidal-Cut Twisted Tape Insert. Int J of Acad Res, 1: 123-128.

17. Murugesan P, Mayilsamy K & Suresh S (2010) Turbulent Heat Transfer and Pressure Drop in a Tube Fitted with Square-Cut Twisted Tape. Chinese J.Chem Eng 18 (4): 609-617.

18. Cui Y & Tian M (2010) Three-Dimensional Numerical Simulation of Thermalhydraulic Performance of a Circular Tube with Edgefold-Twisted-Tape Inserts. J Hydrodyn, 22 (5): 662-670.

19. Guo J, Fan A, Zhang X & Liu W (2011) A Numerical Study on Heat Transfer and Friction Factor Characteristics of Laminar Flow in a Circular Tube Fitted with Center-Cleared Twisted-Tape. Int J Therm Sci, 50: 1263-1270.

20. Zhang X, Liu Z & Liu W (2012) Numerical Studies on Heat Transfer and Flow Characteristics for Laminar Flow in a Tube with Multiple Spaced Twisted Tapes. Int J Therm Sci, 58: 157-167.

21. Salman SD, Kadhum AAH, Takriff MS & Mohamad AB (2014) CFD Simulation of Heat Transfer Augmentation in a Circular Tube Fitted with Alternative Axis Twisted Tape in Laminar Flow under a Constant Heat Flux. Heat Trans Asian Res, 43 (4): 384-396.

22. Chokphoemphun S, Pimsarn M, Thianpong C & Promvonge P (2015) Thermal Performance of Tubular Heat Exchanger with Multiple Twisted-Tape Inserts. Chinenese J Chem Eng, 23: 755-762.

23. Fluent (2006) Fluent 6.3 User's Guide. Lebanon.

24. Versteeg HK & Malalasekera W (2007) An Introduction to Computational Fluid Dynamics- the Finite Volume Method, 2nd Edition. England: Pearson.

25. Yakhot V & Orszag SA (1986) Renormalization Group Analysis of Turbulence I: Basic Theory. J Sci Comput, 1 (1): 1-51.

26. Wilcox DC (1998) Turbulence Modeling for CFD. La Canada, California: DCW Industries Inc.

27. Launder BE & Spaldling DB (1972) Lectures Notes in Mathematical Models of Turbulence. London: Academic Press.

28. Shaw CT (1992) Using Computational Fluid Dynamics. UK: Prentice Hall International Ltd.

29. Gnielinski V (1976) New Equations for Heat and Mass Transfer in Turbulent Pipe and Channel Flow. Int J Chem Eng, 16 (2): 359-368.

30. Seemawute P & Eiamsa-ard S (2010) Thermohydraulics of Turbulent Flow through a Round Tube by Peripherally-Cut Twisted Tape with an Alternate Axis. Int Commun Heat Mass Trans, 37: 652-659.

31. Wongcharee K & Eiamsa-ard S (2011) Friction and Heat Transfer Characteristics of Laminar Swirl Flow through the Round Tubes Inserted with Alternate Clockwise and Counter-Clockwise Twisted-Tapes. Int Commun Heat Mass Trans, 38: 384-352.